IN-26
432258

K. R. Garr,[1] and G. C. Hresko, III,[2]

A Size Effect on the Fatigue Crack Growth Rate Threshold of Alloy 718.

Reference: K. R. Garr, and G. C. Hresko, III, **"A Size Effect on the Fatigue Crack Growth Rate Threshold of Alloy 718,"** *Fatigue Crack Growth Thresholds, Endurance Limits, and Design, ASTM STP 1372*, J. C. Newman, and R.S. Piascik, Eds., American Society for Testing and Materials, West Conshohocken, PA, 1999

Abstract: Fatigue crack growth rate (FCGR) tests were conducted on Alloy 718 in the solution annealed and aged condition at room temperature. In each test, the FCGR threshold was measured using the decreasing ΔK method. Initial testing was at two facilities, one of which used C(T) specimens with W = 127 mm. Previous data at the other facility had been obtained with specimens with W = 50.8 mm. A comparison of test results at R = 0.1 showed that the threshold for the 127 mm specimen was considerably higher than that of the 50.8 mm specimen. A check showed that this difference was not due to a heat-to-heat or lab-to-lab variation. Additional tests were conducted on specimens with W = 25.4 mm and at other R values. Data for the various specimens is presented along with parameters usually used to describe threshold behavior.

Key Words: Alloy 718, crack propagation, crack closure, specimen size effect, fatigue crack growth rate threshold, Biaxiality ratio, T stress, constraint.

Introduction

Two test laboratories were used during the course of obtaining fatigue crack growth rate (FCGR) data on Alloy 718. Considerable testing had been conducted at one facility, laboratory A, on C(T) specimens with a width, W, = 50.8 mm. The second laboratory, laboratory B, used a larger specimen, W = 127 mm.

The FCGR threshold at room temperature with R = 0.1 from laboratory B was considerably higher than the previous values obtained at laboratory A. A heat-to-heat variation was ruled out as the data at laboratory A agreed with data from a different heat of Alloy 718 previously tested at that facility. To check out the potential for a laboratory variation, specimens were exchanged between the two facilities; a 50.8 mm specimen was tested at laboratory B and a 127 mm specimen tested at laboratory A. The results from

---

[1] Engineering Specialist, The Boeing Company, Rocketdyne Propulsion & Power, 6633Canoga Ave., PO Box 7922, Canoga Park, CA 91309-7922.
[2] Associated with Fracture Systems Research, 3135 Essex Road, Allentown, PA 18103

each of these tests agreed with the earlier data based on specimen size. Thus, the disparity in FCGR thresholds could not be attributed to either a heat-to-heat or laboratory variation. Further tests were conducted on specimens with W = 25.4 mm at R = 0.1 and at 0.7 at laboratory A. The report presented here gives the results of the tests conducted at laboratory A on different size specimens at room temperature with additional data from another test series using the same heat of material.

Material

The material tested was Alloy 718 with composition (wt %): C = 0.050, Mo = 2.98, Cr = 18.26, Ni plus Co = 53.40, Ti = 1.00, Al = 0.48, Cb/Ta = 5.10, with the balance being Fe. All specimens were of the C(T) configuration with varying width, W, machined from 12.7 mm plate. They were milled down to the final thickness and electric-discharge machined to the final dimensions with the crack oriented in the T-L direction. The thickness varied slightly. Specimens originally fabricated for laboratory A were roughly 7.6 mm thick while those for laboratory B were about 9.4 mm.

After fabrication, the specimens were given a solution anneal and age heat treatment as follows: solution annealed at 1038 °C for 10 min to 30 min in Argon, followed by an air cool to room temperature. Aged at 760 °C for 10 h, then furnace cooled to 649 °C and held until the total aging plus furnace cooling time equaled 20 h. The average room temperature mechanical properties are: yield strength = 1071.4 MPa, ultimate tensile strength = 1330.7 MPa, elongation = 24 %, and RA = 37.3 %. The grain size taken on specimen 5W1 was ASTM 2.5. It should be pointed out that the specimens for testing at laboratory B were fabricated and heat treated at a different time from the 50.8 mm specimens tested at laboratory A.

Experimental Procedure

The FCGR testing methodology used was in accordance with ASTM Test Method for Measurement of Fatigue Crack Growth Rates (E647-88) except for the pin and clevis arrangement. The 50.8 mm specimens had a 12.7 mm metal bushing inserted in the pin hole with a 9.53 mm diameter pin. The hole in the clevis was standard size but did not have a flat bottom; thus, the hole is oversize for this pin. The 25.4mm specimens had a similar arrangement. The 127 mm specimen used a 25.4 mm diameter pin in a needle roller bearing.

All tests were conducted at room temperature on C(T) specimens with W equal to 25.4 mm, 50.8 mm, and 127 mm. These will be referred to as 1W, 2W, and 5W, respectively, as these represent the relative size variation. Specimens 1W1, 1W2, 1W3, 1W4, 2W1, and 2W5 were electric-discharge machined from the tested halves of specimen 5W1.

Fatigue precracking was performed on all specimens, and the crack growth rate was about 3 X 10^{-6} mm per cycle for specimens tested at R values up to 0.7, below the 10^{-5}

mm per cycle specified in the standard. The highest growth rate recorded was 3.3 X 10^{-5} mm per cycle on a specimen tested at a higher R value.

A closed-loop servo-hydraulic machine was used for all tests. Frequencies in the threshold region were in the range of 100 Hz to 150 Hz. The threshold segment was performed using the automated K-decreasing test procedures [1,2]. Generally, the threshold portion was terminated when the crack growth rate was 1 X 10^{-8} mm/cycle or lower, or the crack showed no further growth after cycling for 12 h to 24 h, indicating that the crack had arrested. This was followed by a K-increasing procedure for verification and to obtain growth rates at higher ΔK's. In some tests a second decreasing ΔK segment was conducted.

Crack length was measured by Direct Current Potential Drop. The current leads were placed at the midpoint of the specimen width, W. The potential leads were on the front face, positioned across the specimen crack mouth. The crack length was related to the normalized change in potential difference by Johnson's equation [3]. All the data, except the closure measurements, were obtained digitally.

A front face clip gage was used to measure crack closure on certain specimens. Frequency was reduced to the 20 to 30 Hz range and the clip gage attached to the specimen. Closure was determined using an oscilloscope. An analog conditioner modified the load and displacement signals to produce a nulled oscilloscope trace that displayed the distinct nonlinear behavior associated with crack closure. Through signal conditioning, the load displacement curve was made to be vertical. This nulled load vs. displacement curve was then amplified and the signal monitored on an oscilloscope. Photographs of the oscilloscope trace were taken with a Polaroid SX 70 camera with automatic exposure. Crack closure levels were determined by visual inspection of the photographs. Typically, closure measurements are taken several times during a test. The load percentage corresponding to the point of non-linearity was entered into the analysis program with the corresponding electric potential value. The analysis program performed a least squares fit to all the closure data and linearly distributed the closure over the FCGR curve.

Data was reduced by the modified secant method. In this method, the Δa and ΔN increments are sequenced to every other data point but incremented by each data point. Successive Δa increments overlap each other. Every point, except the first and last points in a test segment, is used twice. The stress intensity range, ΔK, is calculated from the equation given in the standard using a crack length midway through the increment. The equations for da/dN and a are

$$(da/dN)_i = \frac{[a_{i+1} - a_{i-1}]}{[N_{i+1} - N_{i-1}]} \quad \text{and} \quad a_i = \frac{1}{2}[a_{i+1} + a_{i-1}] \tag{1}$$

where:

$(da/dN)_i$ = crack growth rate of the i^{th} increment

a_i = crack length midway through the increment

N_i = cycle number of the i^{th} increment

Surface roughness measurements were made on several specimens using a Mitutoyo Surftest 402 instrument. Roughness was measured over a 0.762 mm stroke. The instrument was set on either the 10.2 or 50.8 μm range depending on the ability of the instrument to obtain a measurement. Most measurements were made using the 50.8 μm scale. Roughness average was measured which is defined as the arithmetical average of deviations from the center line. Two measurements were taken at each location and the average value used. Measurements were taken at various locations in the central region of the fracture surface with the instrument stroke parallel to the crack growth direction. The specimens were mounted on a movable table with a digital micrometer that was used to set the measurement position. The center of the stroke was used in calculating the roughness position.

Results and Discussion

The da/dN vs. ΔK and ΔK effective curves for specimens tested at R = 0.1 and 0.7 are shown in figures 1a through 1d. The thresholds and other data are given in Table 1. As seen in Fig. 1a and in Table 1, the threshold varies with specimen width. The fatigue crack growth rate (FCGR) curves are independent of specimen size in the high ΔK range. Specimen 5W1 deviates from the group below ΔK of about 30 MPa-$m^{1/2}$ (mid 10^{-5} mm per cycle) whereas the 1W and 2W specimens do not show a difference until the threshold region. Specimen 5W1 has a much higher threshold than the 1W and 2W specimens, well outside the normal scatter for this type of data. A similar result is seen in Fig. 1b for tests at R = 0.7, except that the thresholds for the 1W and 2W specimens are essentially the same. Note, specimen 2W5 was recently tested at Fracture Systems Research and not at laboratory A. Also, the decreasing portion specimen 2W5 was terminated at the value shown without achieving arrest.

Figures 1c and 1d, show the same data plotted as a function of ΔK effective. In Fig. 1c, ΔK effective tends to reconcile the data except near the lowest ΔK effective region. Note, the last point for 2W1 is off the graph, see Table 1. Specimen 5W1 has shifted more than the other specimens.

Figure 1d, shows the data for the R = 0.7 tests. Closure measurements were made on both the 1W specimens but no closure was observed, as noted in Table 1. The 1W data shown are actually ΔK applied for comparison. Specimen 2W5 had a small amount of closure. Specimen 2W5 and 5W2 are in good agreement. Note that closure measurements were made only during the decreasing ΔK segment on specimen 5W2.

Figures 2a and 2b, respectively show the ΔK and K_{max} at thresholds plotted as a function of R. Included are data for 2W specimens of the same heat of material tested at R = 0.4, 0.8, and 0.9 in a different program, none of which had closure measurements taken during the test.

Figure 2a, shows the effect of mean stress on the threshold stress intensity. There is a variation in response of the threshold stress intensity with R that is a function of specimen size, as shown by the different slopes. Included in Fig. 2a are the ΔK effective thresholds.

Table 1 Summary of Threshold Data

Specimen	Width (mm)	Thickness (mm)	R	Applied ΔK(th) (MPa-$m^{1/2}$)	da/dN at Threshold (mm/cy)	Effective ΔK(th) (MPa-$m^{1/2}$)	a at Threshold (mm)	a/W at Threshold	C (mm^{-1})
1W1	25.425	9.398	0.1	6.54	8.94×10^{-9}	1.88	9.789	0.385	-0.20
1W2	25.349	9.423	0.1	6.56	7.80×10^{-9}	1.86	9.708	0.383	-0.20
2W1	50.825	9.398	0.1	10.13	7.87×10^{-8}	2.45	15.796	0.311	-0.08
2W1 (a)	50.825	9.398	0.1	7.79	1.04×10^{-8}	0.97	25.842	0.508	-0.08
2W2	50.698	7.747	0.1	9.86	6.30×10^{-8}		17.943	0.354	-0.08
2W3	50.698	7.823	0.1	9.13	4.78×10^{-9}		18.636	0.368	-0.08
5W1	126.873	9.271	0.1	15.37	4.67×10^{-8}	1.30	36.695	0.289	-0.08
5W1 (a)	126.873	9.271	0.1	17.72	1.18×10^{-7}	2.78	45.095	0.355	-0.08
2W4	50.749	7.747	0.4	7.60	3.94×10^{-8}		18.306	0.361	-0.08
2W4 (a)	50.749	7.747	0.4	6.05	2.43×10^{-8}		27.658	0.545	-0.08
1W3	25.375	9.398	0.7	3.00	3.81×10^{-9}	(b)	12.377	0.488	-0.20
1W4	25.425	9.423	0.7	2.78	9.14×10^{-9}	(b)	14.059	0.553	-0.08
2W5 (c)	50.775	9.423	0.7	3.07	1.58×10^{-8}	1.80	25.784	0.508	-0.08/-0.16
2W6	50.698	7.849	0.7	3.15	6.10×10^{-9}		25.517	0.503	-0.08
2W7	50.724	7.823	0.7	2.69	1.38×10^{-8}		26.861	0.530	-0.08
5W2	126.949	9.550	0.7	4.48	5.41×10^{-9}	1.91	36.101	0.284	-0.08
2W8	50.724	7.569	0.8	2.85	2.05×10^{-9}		27.318	0.539	-0.08
2W9	50.876	7.696	0.9	2.51	5.28×10^{-9}		20.610	0.405	-0.08
2W10	51.054	7.798	0.9	3.30	8.97×10^{-9}		17.318	0.339	-0.08

(a) Indicates a second decreasing ΔK test on the same specimen.

(b) Closure measurements were taken, however, no evidence of closure was found in this specimen.

(c) No arrest; decreasing segment terminated at threshold value shown. Last 11 points were with the steeper gradient.

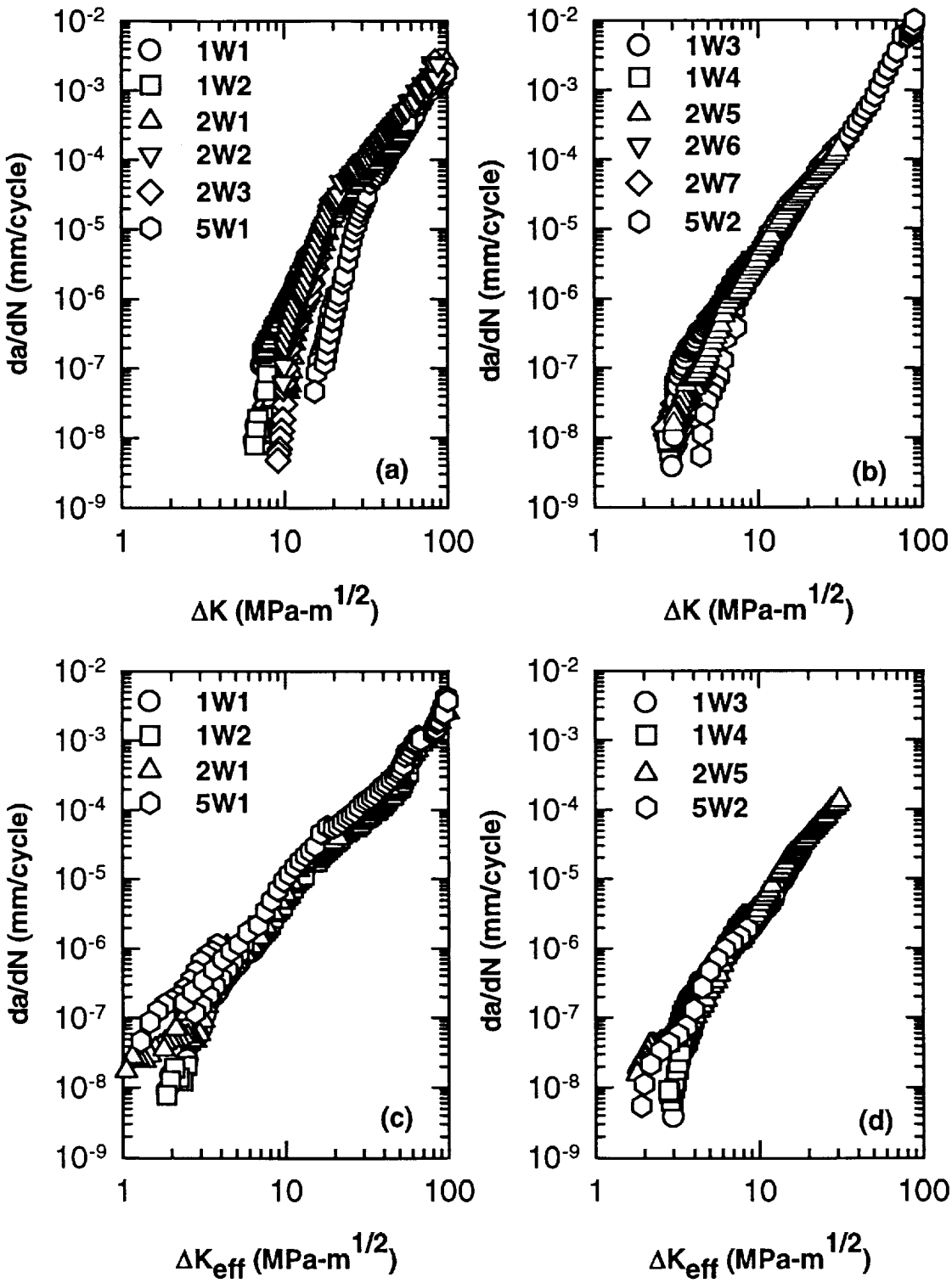

Figure 1: (a) da/dN vs. ΔK for R = 0.1, (b) da/dN vs. ΔK for R = 0.7, (c) da/dN vs. ΔK effective for R = 0.1, (d) da/dN vs. ΔK effective for R = 0.7 except 1W specimens are vs. ΔK.

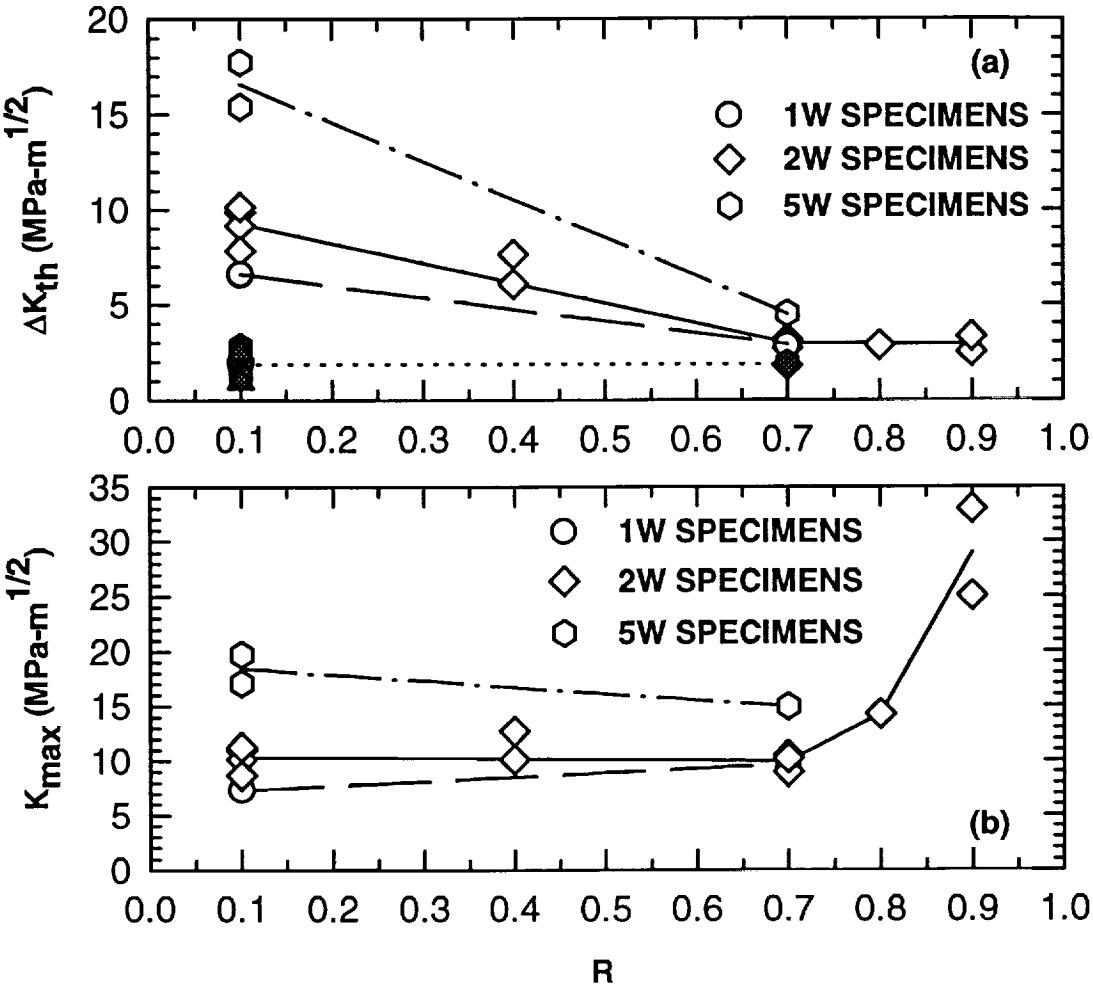

Figure 2. (a) ΔK_{th} vs. R. Open symbols are ΔK applied. Closed symbols are ΔK effective, (b) K_{max} vs. R. All data are at threshold.

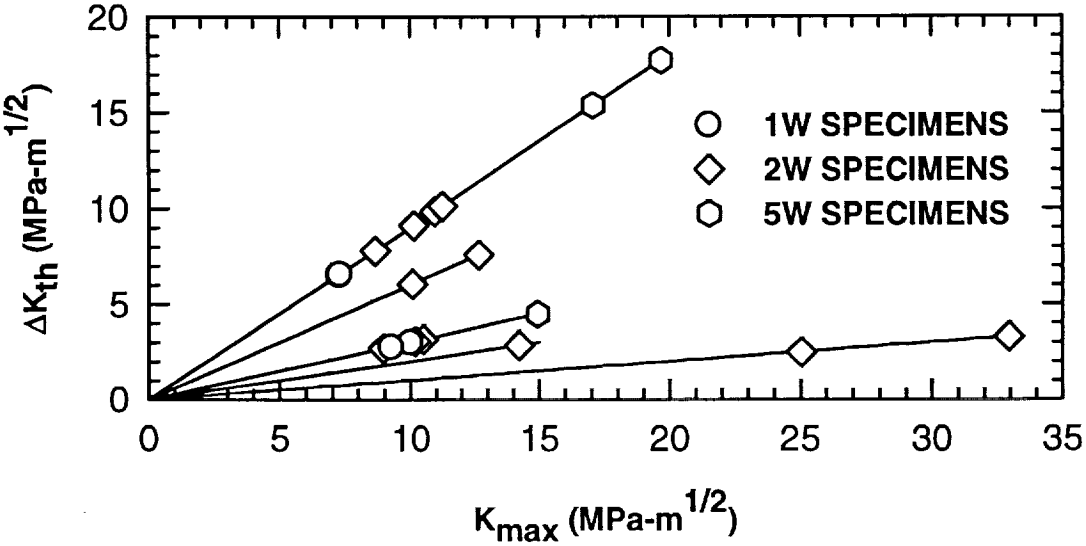

Figure 3. ΔK_{th} vs. K_{max}.

The ΔK effective thresholds appear to be independent of mean stress and specimen size.

The lines drawn in Fig.2a are from the average value of the threshold at R = 0.1 to the average value at R = 0.7. For the 2W specimens, the line then connects to the average of the 0.9 data. The data at R = 0.4 and 0.8 were not used in determining the lines.

Figure 2b shows K_{max} vs. R at threshold confirming the observations made in Fig. 2a. Figures 2a and 2b indicate that the region controlled by K_{max} and ΔK vary with specimen size. In Fig 2b, the 5W specimens have a negative slope between R = 0.1 and 0.7 while the 1W specimens have a positive slope.

As closure was not found in the 1W specimens, it is possible that the transition from K_{max} to ΔK control is at an R value lower than 0.7. Assuming that the value of threshold at R = 0.6 is the same as at R = 0.7 would produce the same value of Kmax at both R = 0.1 and 0.6. This would produce a zero slope line in Fig. 2b with the transition from K_{max} to ΔK control at R = 0.6. It would also make the slope of the 1W line in Fig.2a slightly steeper. Rectifying the 5W data requires an increase in the average value of the R = 0.7 threshold. More data with closure are needed for different size specimens at different R values.

Doker, et. al., [4] appears to have first suggested plotting threshold data as ΔK_{th} vs. K_{max}. More recently in a series of papers, Vasudevan, et al [5,6] and Sadananda and Vasudevan [7] expanded the use of the two parameter approach. Figure 3 is a plot of ΔK_{th} vs. K_{max}. The data for the different size specimens tested at the same R value fall on the same line. All the same R value data fall on their respective lines with slopes of (1-R). The lowest ΔK_{th} value is 2.51 MPa-$m^{1/2}$ for the 2W specimen at R = 0.9. This is ΔK^*_{th} according to their nomenclature. Based on the trend of the data in Fig. 2a, this value appears to be independent of specimen size. Although negative R value tests were not conducted, it appears that the lowest K_{max}, K^*_{max}, would depend on specimen size.

An estimate of the K^*_{max} for each specimen size was made. For each specimen size, the lowest threshold at R = 0.1 and the highest threshold at R = 0.7 were used to estimate the lowest threshold at R = 0. Using data given by Usami [8], an estimate of the ΔK_{th} at R = -1 was made and K_{max} calculated. The K_{max} values for the 1W, 2W, and 5W specimens are 6.21, 7.46, and 14.97 MPa-$m^{1/2}$, respectively. According to Vasudevan, et al [5,6] and Sadananda and Vasudevan [7], the region below the limiting values of ΔK^*_{th} and K^*_{max} should not produce crack growth. Based on this, the 5W data would not have predicted crack growth at the values observed in the 1W and 2W specimens, and the 2W data would not have predicted the 1W data, tested at R equal to 0.1.

Figure 4a through 4c shows the trend in closure level, $U = \Delta K_{eff}/\Delta K$, as a function of various parameters. Figure 4a and 4b show only the decreasing ΔK data while 4c includes the increasing ΔK data. The shaded symbols represent R = 0.7 data, the open symbols are for R = 0.1 data. Figure 4a shows U as a function of ΔK. In all cases the fraction of the load cycle over which the crack is open decreases as threshold is approached, i.e., closure increases. For the R equal to 0.1 data, the closure levels follow the specimen size with the larger the size having the higher closure level.

This result is consistent with those of Zawada and Nicholas [9]. They tested C(T) specimens of Rene 95 of different sizes at 650°C in vacuum and lab air at R = 0.1 in the near threshold region. They also tested at different values of C, the load shedding

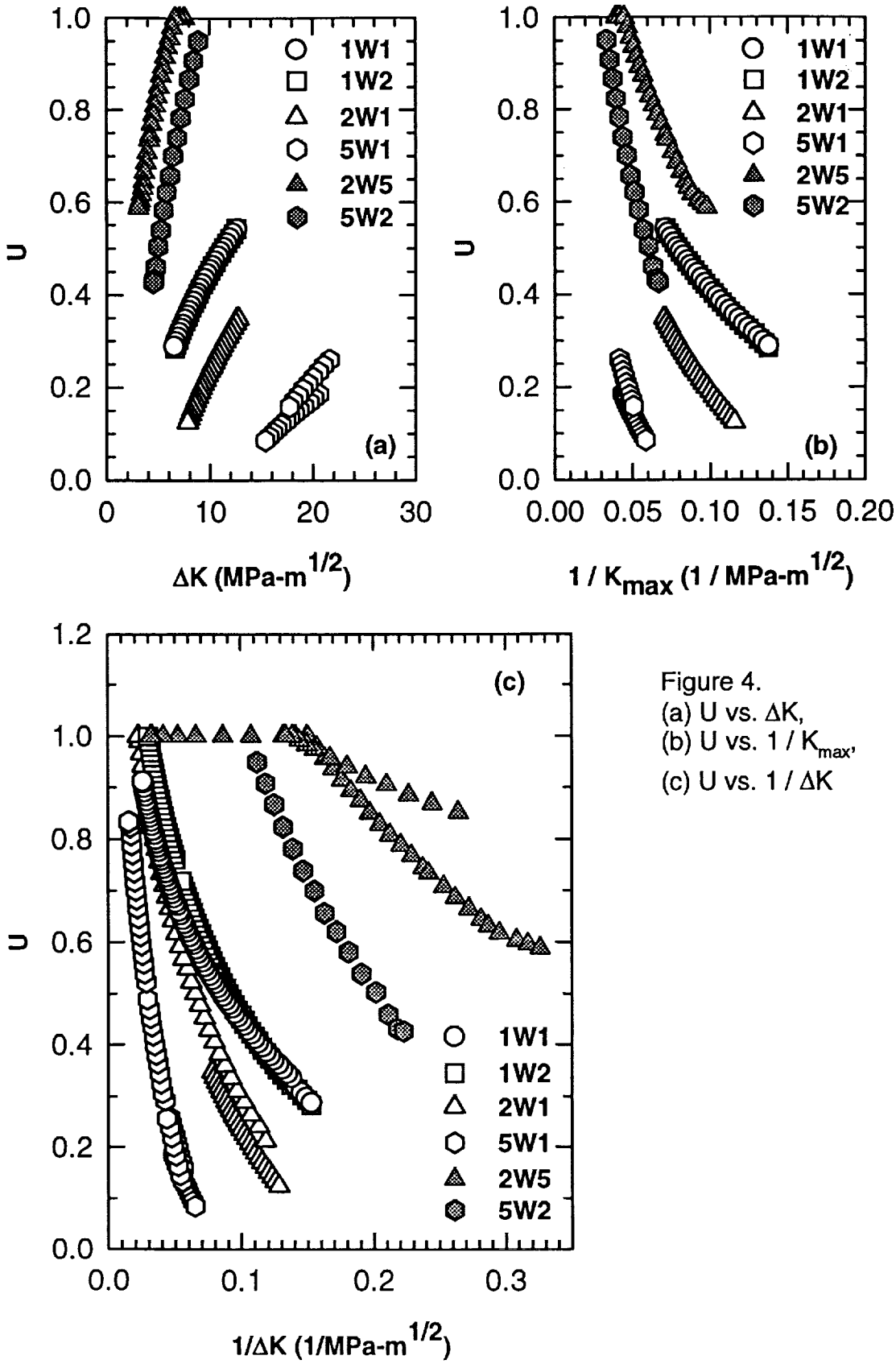

Figure 4.
(a) U vs. ΔK,
(b) U vs. 1 / K_{max},
(c) U vs. 1 / ΔK

constant. Their results showed no effect of the load shedding constant between –0.08 and $-1.2\ mm^{-1}$. Their results also showed no effect of thickness for W = 40 mm with thickness equal to 5 mm and 10 mm. They did, however, observe a difference in the closure level between the W = 40 mm and 20 mm specimens with thickness equal to 5 mm. The smaller specimen had lower values of K_{cl}. Zawada and Nicholas [9] considered the difference in closure levels between the two sizes to be outside the "specimen-to-specimen variability" and "beyond the uncertainty in determining closure loads".

In a study of the effect of load history and specimen geometry on the value of the crack closure load, Ashbaugh [10] observed a size effect. Crack closure was measured by CMOD, back face strain gage, and interferometric displacement gage (IDG) on three different size C(T) specimens. Two specimens had W = 40 mm, one with B = 10 mm (standard) and the other with B = 5 mm (thin), and one specimen with W = 20 mm and B = 5 mm (half size). Ashbaugh tested Rene 95 at room temperature and R = 0.1. In constant amplitude tests, the half size specimen had lower values of K_{cl} than did the standard and thin specimens, which were essentially the same. The difference in closure levels was considered to be outside the normally observed scatter in the data by Ashbaugh [10].

The results shown in Fig. 4a are in agreement with the data of Shercliff and Fleck [11] on BS 4360 50B steel. The increase in R value for the 5W specimens increased da/dN, see Fig. 1, and increased U. They attributed the near threshold behavior to oxide or roughness induced closure.

Hudak and Davidson [12] found that a plot of U vs. 1/Kmax linearized the data over a wide range of R values for 7091 Al (R = 0.1 to 0.8) and for 304 stainless steel (R = 0.1 to 0.7). They used a special technique that measured the closure locally, at the crack tip. Hudak and Davidson [12] were also able to fit the 7091 Al threshold data of Minakawa and McEvily [13].

Minakawa and McEvily's data [13] where in the near threshold region at R = 0.05 with closure measured using a front face clip gage. They originally plotted K_{op}/K_{max} as a function of ΔK which showed a nonlinearity. Our data, see Fig. 5a, also shows a non-linearity when plotted in that way. However, our data, Fig. 4b, also shows some non-linearity in the lower $1/K_{max}$ region. A plot, not shown, of U vs. $1/K_{max}$ which includes the increasing ΔK region shows a continuation of the nonlinearity. Note that R = 0.1 and 0.7 data for the 5W specimens do not match up.

Davidson [14] measured the closure by a stereo technique that allowed him to determine the mode I and mode II closure levels. He plotted U vs. $1/\Delta K$ and showed that the opening load in mode II was lower than in mode I at low values of ΔK. The mode I closure was linear while the mode II closure was nonlinear in the low ΔK region. Figure 4c is a plot of our data that also includes the increasing ΔK region. However, our closure measurements do not differentiate between mode I and mode II closure. The threshold data are at the high end of the $1/\Delta K$ range. Note that specimen 5W2 is all threshold data.

The main point of figure 4 is that different size specimens have different amounts of closure at the same value of ΔK. A plot of U vs. a / W, not shown, does not consolidate the data.

Figures 5a and 5b show K_{op}/K_{max} vs. ΔK or K_{max}, respectively, exhibit again that

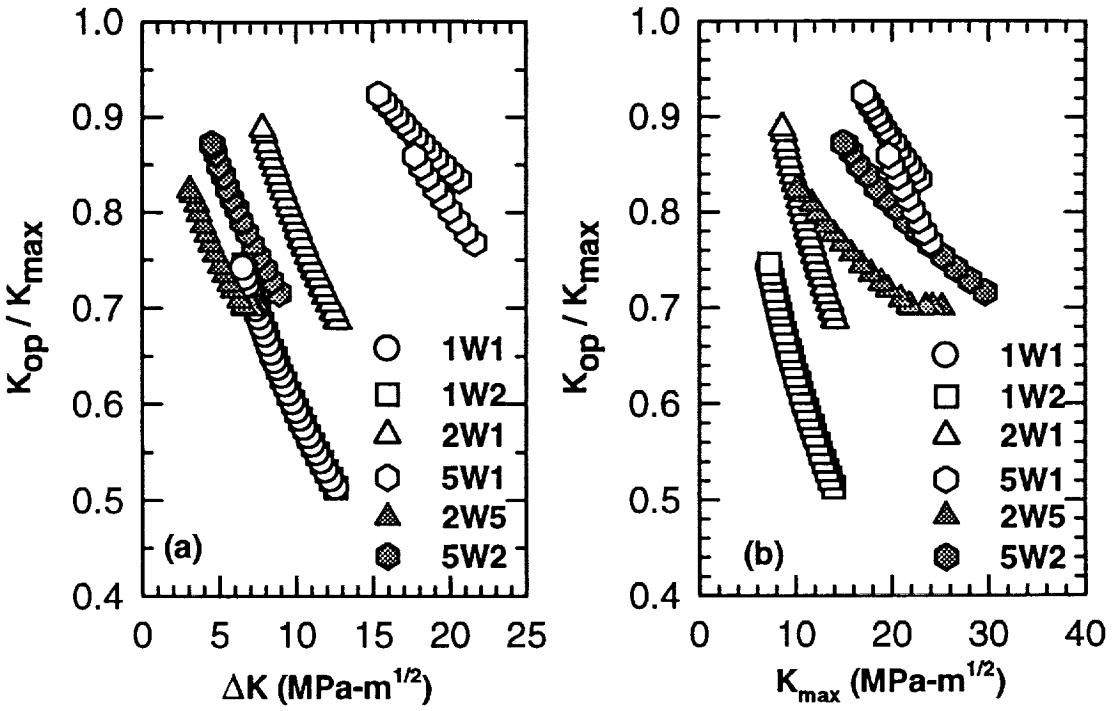

Figure 5. (a) K_{op} / K_{max} vs. ΔK, (b) K_{op} / K_{max} vs. K_{max}.

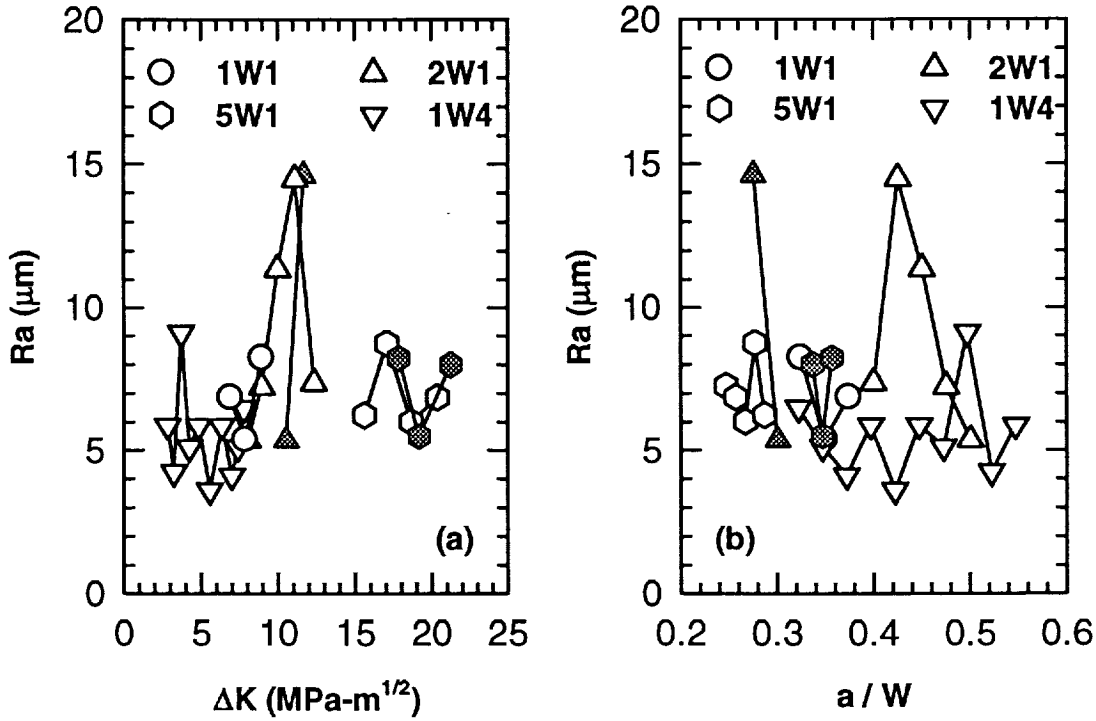

Figure 6. Roughness measurements (a) vs.ΔK and (b) vs. a / W. Measured parallel to the growth direction. Closed symbols are for the decreasing ΔK mode with the higher threshold.

closure increases with specimen size. Considering Fig. 5a, Shercliff and Fleck [11] observed a similar behavior in the 6082 Al they tested and attributed this to roughness induced closure.

To summarize the results, the threshold and the degree of closure vary with specimen size. The question is what causes the differences?

Several parameters were investigated in an attempt to answer that question. The plastic zone size, the biaxiality ratio (B), the T stress, and the specimen roughness. Table 2 gives the plastic zone size, PZS, divided by the specimen thickness, t, and PZS divided by the remaining ligament, (W-a), at the start of the decreasing ΔK segment and at threshold. Also included in the table are values of B and T at the start and at the threshold. The plastic zone size, PZS, was calculated using the equation

$$PZS = (1/2\pi)(\frac{K\,\max}{\sigma_y})^2 \qquad (2)$$

where

σ_y = yield strength

As seen in Table 2, the value of PZS/thickness increases with specimen size for specimens tested at R = 0.1, compare specimens 1W1, 1W2, 2W1, and 5W1. This holds for both at the start and at threshold. This trend does not appear to hold for specimens tested at R = 0.7, compare specimens 1W3, 1W4, 2W5, and 5W2. The reverse trend occurs when PZS/(W-a) is compared. Here the larger specimens have the smaller value, particularly at the start. Newman [15] stated that as long as the PZS divided by crack length and PZS divided by the remaining ligament are less than 0.1, small scale yielding conditions exist. All the specimens met this criteria.

Leevers and Radon [16] gave values of B, the biaxiality ratio, for the C(T) configuration as a function of a/W. Their Case b data were fitted to a 5^{th} order polynomial and the coefficients used to calculate B at the start and at threshold. As all the specimens started the first decreasing ΔK section at an a/W of about 0.25, there was essentially no variation in B. Also, most of the specimens reached threshold at a/W of between 0.35 and 0.4, again producing little variation in B. Only those specimens that had a second decreasing ΔK segment had larger values of B.

The equation used to calculate the T stress was that given by Leevers and Radon [16] with K_{max} being used in all cases. The T stress showed some variation; the largest values being for the specimens tested at the high R values.

Roughness measurements were taken on several specimens. Figure 6 shows the roughness variation for specimens on which closure was measured. The data shown are only for the decreasing ΔK segments. Although there is considerable variation in the roughness of an individual specimen, most of the measurements were in the 4 to 9 μm range independent of size or R value. The roughness of the specimens originally

Table 2. Summary of Various Parameters at the Start of a Decreasing ΔK Segment and at Threshold

Specimen	R	PZS/t Start	PZS/t at ΔKth	PZS/ (W-a) at Start	PZS/ (W-a) at ΔKth	B at Start (b)	B at ΔKth (b)	T at Start (MPa)	T at ΔKth (MPa)
1W1	0.1	2.89×10^{-3}	7.79×10^{-4}	1.44×10^{-3}	4.68×10^{-4}	0.344	0.523	33.61	21.68
1W2	0.1	2.88×10^{-3}	7.82×10^{-4}	1.44×10^{-3}	4.71×10^{-4}	0.342	0.521	33.44	21.75
2W1	0.1	2.91×10^{-3}	1.87×10^{-3}	7.25×10^{-4}	5.02×10^{-4}	0.342	0.429	23.77	21.69
2W1 (a)	0.1	2.97×10^{-3}	1.11×10^{-3}	9.06×10^{-4}	4.16×10^{-4}	0.531	0.599	30.11	18.20
2W2	0.1	4.59×10^{-3}	2.15×10^{-3}	9.49×10^{-4}	5.08×10^{-4}	0.349	0.488	27.44	22.51
2W3	0.1	4.57×10^{-3}	1.82×10^{-3}	9.48×10^{-4}	4.45×10^{-4}	0.342	0.504	27.18	21.14
5W1	0.1	7.85×10^{-3}	4.36×10^{-3}	7.71×10^{-4}	4.49×10^{-4}	0.341	0.396	24.47	19.93
5W1 (a)	0.1	8.62×10^{-3}	5.80×10^{-3}	9.49×10^{-4}	6.58×10^{-4}	0.465	0.490	30.51	25.63
2W4	0.4	6.74×10^{-3}	2.87×10^{-3}	1.39×10^{-3}	6.86×10^{-4}	0.343	0.496	32.91	26.22
2W4 (a)	0.4	6.48×10^{-3}	1.82×10^{-3}	1.63×10^{-3}	6.11×10^{-4}	0.533	0.603	40.42	20.64
1W3	0.7	1.24×10^{-2}	1.48×10^{-3}	6.40×10^{-3}	1.07×10^{-3}	0.384	0.593	74.38	30.09
1W4	0.7	1.33×10^{-2}	1.26×10^{-3}	6.60×10^{-3}	1.05×10^{-3}	0.339	0.603	71.37	26.59
2W5	0.7	9.33×10^{-3}	1.53×10^{-3}	2.34×10^{-3}	5.78×10^{-4}	0.347	0.599	42.97	21.48
2W6	0.7	1.59×10^{-2}	1.95×10^{-3}	3.32×10^{-3}	6.08×10^{-4}	0.343	0.598	50.90	22.20
2W7	0.7	1.35×10^{-2}	1.43×10^{-3}	2.79×10^{-3}	4.68×10^{-4}	0.341	0.602	46.53	18.60
5W2	0.7	1.28×10^{-2}	3.24×10^{-3}	1.26×10^{-3}	3.41×10^{-4}	0.306	0.388	29.61	17.24
2W8	0.8	3.49×10^{-2}	3.71×10^{-3}	7.03×10^{-3}	1.20×10^{-3}	0.344	0.603	74.17	29.28
2W9	0.9	3.27×10^{-2}	1.13×10^{-2}	6.88×10^{-3}	2.88×10^{-3}	0.382	0.543	76.90	53.43
2W10	0.9	3.17×10^{-2}	1.93×10^{-2}	6.73×10^{-3}	4.47×10^{-3}	0.383	0.469	76.17	66.30

(a) Indicates a second decreasing ΔK test on the same specimen.

(b) $B = -0.209+2.758\alpha-4.479\alpha^2+15\alpha^3-32.083\alpha^4+21.667\alpha^5$.

Where $\alpha = a/W$

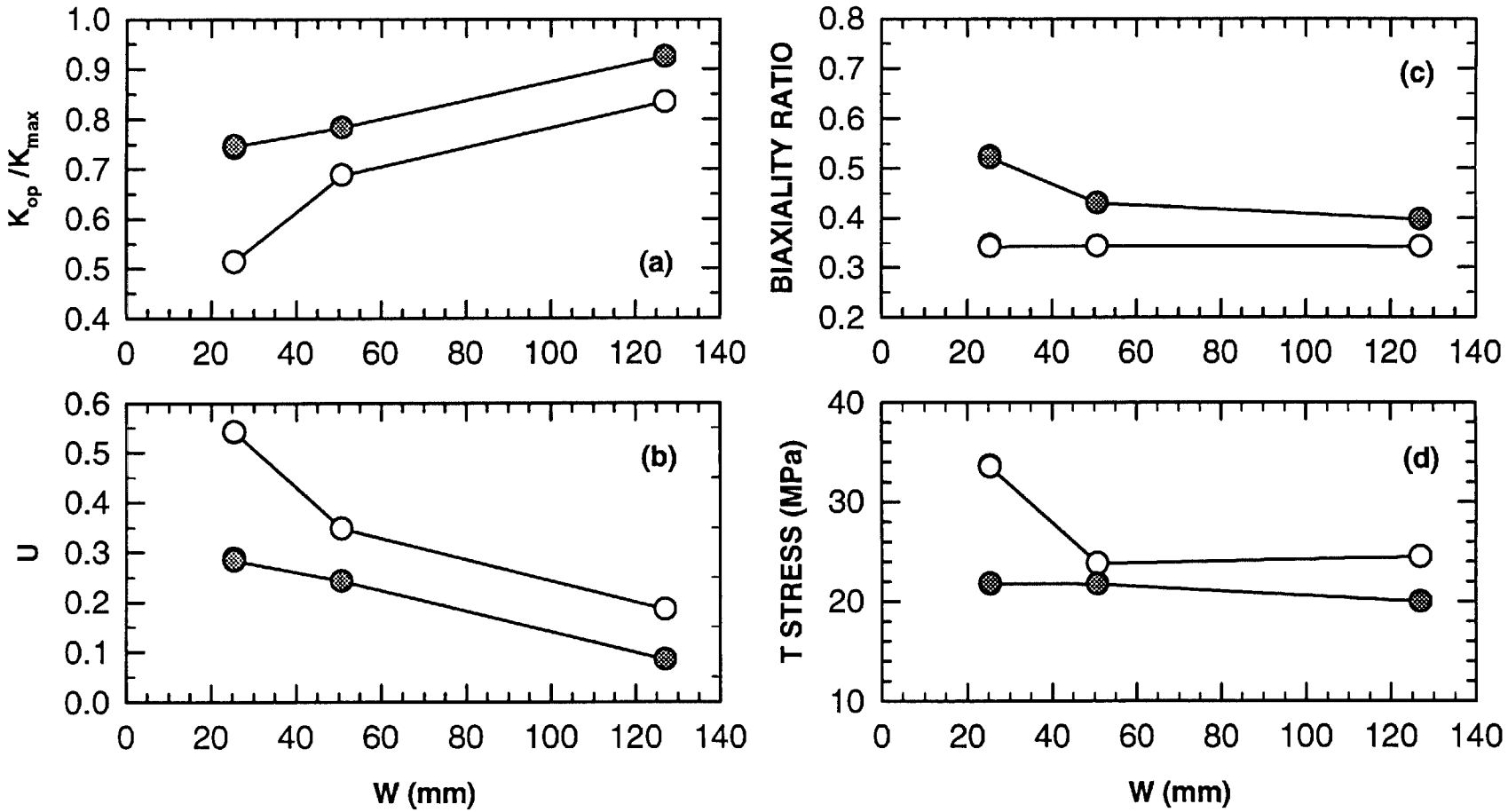

Figure 7. (a) Kop / Kmax vs W, (b) U vs. W, (c) Biaxiality ratio vs. W, (d) T stress vs. W. Open symbols are at start, closed symbols are at threshold. Data for 50.8 and 127 mm specimens are for the first threshold segment. All data are for R = 0.1.

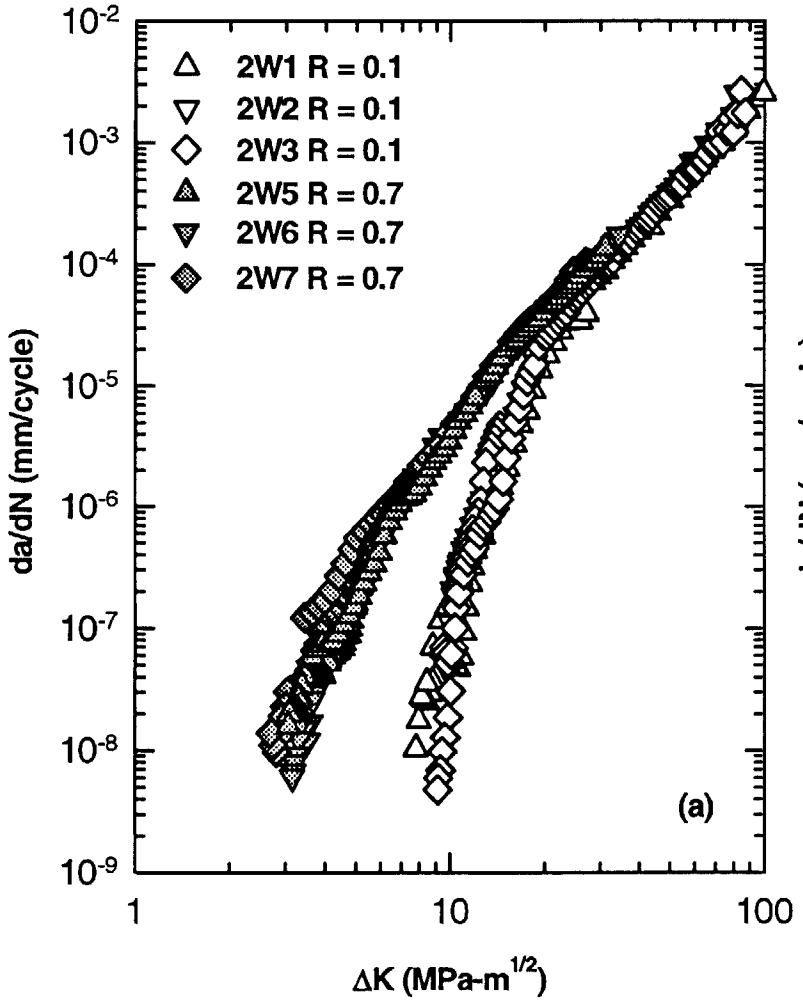

Figure 8a. da/dN vs. ΔK for 2W Specimens

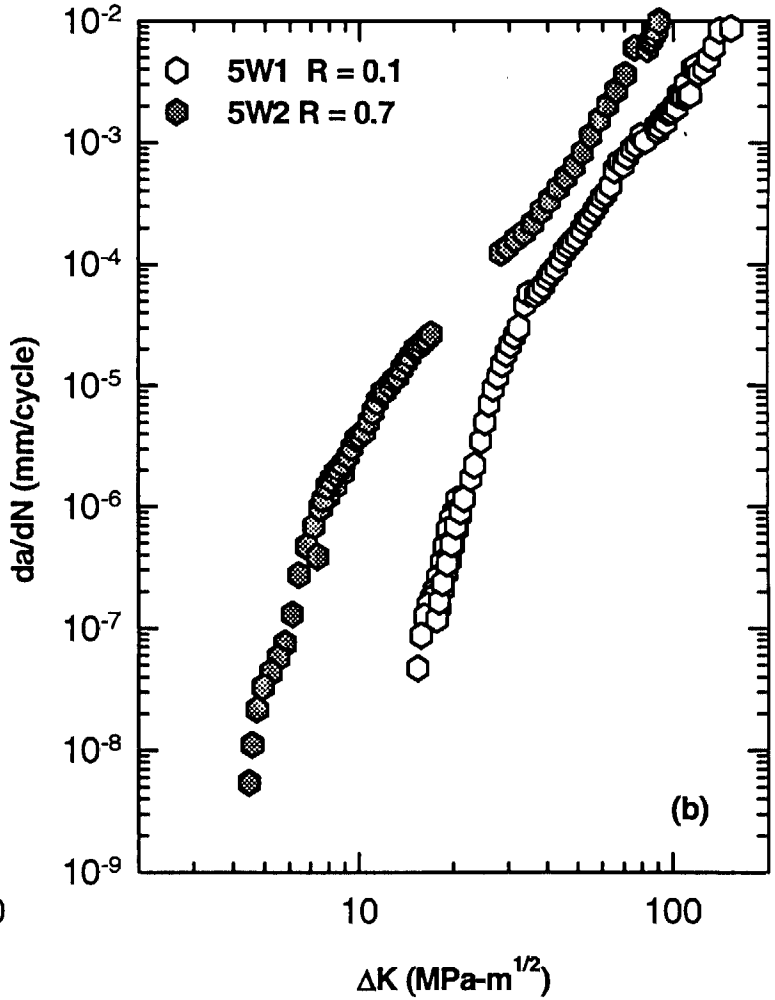

Figure 8b. da/dN vs. ΔK for 5W Specimens

fabricated for testing at laboratory A have essentially the same roughness range, 4 to 10 μm regardless of R value.

Figure 7 shows the trend in some of the parameters investigated as a function of specimen width for specimens tested at R = 0.1. In Fig. 7a, K_{op}/K_{max} increases with W with the commensurate decrease in U, Fig. 7b. Figure 7c shows the biaxiality ratio. The variation in the value at ΔK_{th} is due to the variation in a/ W at threshold The T stress, Fig. 7d, shows some variation at the start of the test but very little at threshold.

Constraint was also considered as a possible reason for the difference in threshold with specimen size. Fig. 8a and 8b show da/dN vs. ΔK for the 2W and 5W specimens tested at R = 0.1 and 0.7, respectively. In Fig. 8a, note that a very small shift in the R = 0.7 curve would bring the Paris section in line with the Paris region of the R = 0.1 curve. In Fig. 8b, for the 5W specimens, a much larger separation is seen. Newman's closure model [17] with the maximum stress divided by the flow stress, S_{max}/σ_o, of 0.2 was used to estimate the Paris region constraint factor. The constraint factor, α, was 3 for the 1W and 2W specimens and 1.2 for the 5W specimens. Newman's model is based on plasticity and applies to the Paris region and is not applicable to the threshold region. Also, in these tests the Paris region is obtained after the threshold has been determined and thus, can't influence directly the threshold behavior. However, it is included here as it gives an indication that the constraint is different in the larger specimen and that constraint may be a factor in controlling the threshold behavior. At present the authors are not aware of a constraint model for the threshold region for nickel base superalloys.

Some speculation by the authors is offered. Roughness is essentially the same regardless of specimen size and the R value tested. Assuming that the curvature seen in Fig. 4c is indicative of mode II, as seen by Davidson [14], a possible explanation for the different thresholds is that the amount of mode II in a specimen is a function of size. An alternative explanation may be made on the basis of the difference in constraint with specimen size, as seen in Fig. 8.

Conclusion

Fatigue crack growth rate tests were conducted on Alloy 718 at room temperature at R = 0.1 and 0.7 on C(T) specimens with W of 25.4 mm, 50.8 mm, and127 mm. Additional data on 50.8 mm specimens was obtained from a separate test program. The FCGR threshold varied with specimen width, particularly at R = 0.1, with the highest threshold being for the 127 mm specimen. Closure was measured on some specimens and the ΔK effective threshold obtained. Although this was instrumental in reconciling the data, it did not explain why there is more closure in the larger specimen. The biaxiality ratio and T stress were calculated but did not show a significant difference that could explain the data. Roughness measurements were taken on specific specimens, again with no significant difference between the specimens. Most of the roughness measurements were between 4 and 10 μm regardless of R value or specimen size. At this time there does not appear to be an obvious explanation for the different thresholds due to the specimen size. Constraint or mode II behavior are possible mechanisms that may explain the differences. Additional

FCGR data are needed over a wide range of R values and specimen sizes to better describe the boundary of the size effect and the variables controlling the behavior.

Acknowledgments

This paper is based on work performed under NASA Contracts NAS8-40000 and NAS8-45000. We are pleased to acknowledge the contribution of P. Stirling for fractography, the assistance of R. Ball with the roughness measurements, and the helpful discussions with J. C. Newman, Jr. and D. Russell.

References

[1] Saxena, A., Hudak, Jr., S. J., Donald, J. K., and Schmidt, D. W., "Computer-Controlled Decreasing Stress Intensity Technique for Low Rate Fatigue Crack Growth Testing," *Journal of Testing and Evaluation*, Vol. 6, No. 3, 1978, pp. 167-174.

[2] Donald, J. K., and Schmidt, D. W., "Computer-Controlled Stress Intensity Gradient Technique for High Rate Fatigue Crack Growth Testing," *Journal of Testing and Evaluation*, Vol. 8, No. 1, Jan. 1980, pp. 19-24.

[3] Schwalbe, K. H. and Hellmann, D., "Applicationof the Electrical Potential Method to Crack Lengths Measurements Using Johnson's Formula," *Journal for Testing and Evaluation*, Vol. 9, No. 3, May 1981, pp. 218-221.

[4] Doker, H., Bachmann, V., and Marci, G., "A Comparison of Different Methods of Determination of the Threshold for Fatigue Crack Propagation", *Fatigue Thresholds, Vol. I*, J. Backlund, A. F. Blom, and C. J. Beevers, Eds. Engineering Materials Advisory Services, Inc., Warley, West Midlands, United Kingdom, 1982, pp.45-57.

[5] Vasudeven, A. K., Sadananda, K., and Louat, N., "Two Critical Stress Intensities for Threshold Fatigue Crack Propagation", *Scripta Metallurgica et Materialia*, Vol. 28, 1993, pp. 65-70.

[6] Vasudeven, A. K., Sadananda, K., and Louat, N., "A Review of Crack Closure, Fatigue Crack Threshold and Related Phenomena", *Material Science and Engineering*, Vol. A188, 1994, pp. 1-22.

[7] Sadananda, K. and Vasudeven, A. K., "Analysis of Fatigue Crack Closure and Thresholds," *Fracture Mechanics: 25th Volume, ASTM STP 1220*, F. Erodgan, Ed., American Society for Testing and Materials, Philadelphia, 1995, pp. 484-501.

[8] Usami, S., "Applications of Threshold Cyclic-Plastic-Zone-Size Criterion to some Fatigue Limit Problems", *Fatigue Thresholds, Vol. I*, J. Backlund, A. F. Blom, and C. J. Beevers, Eds. Engineering Materials Advisory Services, Inc., Warley, West Midlands, United Kingdom, 1982, pp.205-238

[9] Zawada, L. P. and Nicholas, T., "The Effect of Closure on the Near-Threshold Fatigue Crack Propagation Rates of a Nickel Base Superalloy," *Mechanics of Fatigue Crack Closure, ASTM STP 982*, J. C. Newman, Jr. and W. Elbers, Eds. American Society for Testing and Materials, Philadelphia, 1988, pp. 548-567.

[10] Ashbaugh, N. E., "Effects of Load History and Specimen Geometry on Fatigue Crack Closure Measurements," *Mechanics of Fatigue Crack Closure, ASTM STP 982*, J. C. Newman, Jr. and W. Elbers, Eds. American Society for Testing and Materials, Philadelphia, 1988, pp. 186-189.

[11] Shercliff, H. R., and Fleck, N. A., "Effect of Specimen Geometry on Fatigue Crack Growth in Plane Strain-I. Constant Amplitude Response.", *Fatigue and Fracture of Engineering Materials and Structures"*, Vol.13, 1990, pp. 287-296.

[12] Hudak, S. J., and Davidson, D. L., "The Dependence of Crack Closure on Fatigue Loading Variables" *Mechanics of Fatigue Crack Closure, ASTM STP 982*, J. C. Newman, Jr. and W. Elbers, Eds. American Society for Testing and Materials, Philadelphia, 1988, pp. 121-138.

[13] Minakawa, K., and McEvily, A. J., "On Crack Closure in the Near-Threshold Region", *Scripta Metallurgica,* Vol. 15, 1981, pp. 633-636.

[14] Davidson, D. L., "Plasticity Induced Fatigue Crack Closure," *Mechanics of Fatigue Crack Closure, ASTM STP 982*, J. C. Newman, Jr. and W. Elbers, Eds. American Society for Testing and Materials, Philadelphia, 1988, pp. 186-189.

[15] Newman, J. C. Jr., "Prediction of Stable Crack Growth and Instability Using the V_R-Curve Method", *Elastic-Plastic Fracture Mechanics Technology, ASTM STP 896*, J. C. Newman, Jr., and F.J. Loss, Eds., American Society for Testing and Materials, Philadelphia, 1985, pp. 135-166.

[16] Leevers, P. S. and Radon, J. C., "Inherent Stress Biaxiality in Various Fracture Specimen Geometries", *International Journal of Fracture*, Vol. 19, 1982, pp. 311-325.

[17] Newman, J. C. Jr., "A Crack Opening Stress Equation for Fatigue Crack Growth", *International Journal of Fracture*, Vol. 24, 1984, pp. R131-R135.